Modelling performance of two- and four-terminal thin-film silicon tandem solar cells under varying spectral conditions

Reynolds, Stephen; Smirnov, Vladimir

Published in:
Energy Procedia

DOI:
10.1016/j.egypro.2015.12.321

Publication date:
2015

Document Version
Publisher's PDF, also known as Version of record

Available online at www.sciencedirect.com

ScienceDirect

Energy Procedia 84 (2015) 251 – 260

Energy Procedia

E-MRS Spring Meeting 2015 Symposium C - Advanced inorganic materials and structures for photovoltaics

Modelling performance of two- and four-terminal thin-film silicon tandem solar cells under varying spectral conditions

Steve Reynolds[a,*], Vladimir Smirnov[b]

[a]*University of Dundee, School of Science and Engineering, Dundee DD1 4HN, U.K.*
[b]*IEK-5 Photovoltaik, Forschungszentrum Jülich, D-52425 Jülich, Germany*

Abstract

In an amorphous silicon/microcrystalline silicon or 'micromorph' tandem solar cell, variations in solar spectral quality alter the proportion of photo-generated current developed by each sub-cell. This imbalance may reduce long-term energy conversion efficiency, compared with operation under a constant AM1.5G spectrum. Using semi-empirical modelling, we contrast the usual series-connected two-terminal tandem cell, constrained by current-matching, with a four-terminal tandem cell, in which both sub-cells are electrically independent. The model reveals that reduction in extracted power due to current mismatch in two-terminal connection is compensated somewhat by an increase in fill-factor either side of the current-matched point. The efficiency-mismatch curve is compared with spectral distributions of annual insolation in terms of average photon energy. Provided the two-terminal cell is matched to the prevailing spectral distribution, long-term benefits in electrical energy output in four-terminal connection are predicted to be modest. However departures from the AM1.5G spectrum occur worldwide, and this plus the flexibility to match to seasonal degradation/annealing cycles suggests that four-terminal connection may offer greater benefit.

Peer-review under responsibility of The European Materials Research Society (E-MRS)

Keywords: tandem solar cells; computer modelling; solar spectrum; current matching

1. Introduction

'Micromorph' tandem solar cells comprising amorphous silicon (a-Si:H) top-cell – microcrystalline silicon (μc-Si:H) bottom-cell [1] enable higher photovoltaic (PV) conversion efficiencies to be achieved in comparison with

* Corresponding author. Tel.: +44(0)1382 384559; fax: +44(0)1382 384389.
E-mail address: s.z.reynolds@dundee.ac.uk

Peer-review under responsibility of The European Materials Research Society (E-MRS)
doi:10.1016/j.egypro.2015.12.321

equivalent single-junction cells, due primarily to more effective spectral matching and reduced thermalisation loss [2] and improved resistance to light-induced degradation [3]. Top and bottom sub-cells are normally internally series-connected as a natural consequence of the deposition process, to give a *two-terminal* (2T) device, as shown in Fig. 1(a). However 2T connection imposes a limiting boundary condition – that the currents in both sub-cells must remain equal. To achieve optimal power transfer therefore requires careful tuning of photogenerated currents, *e.g.* by adjustment of absorber-layer thicknesses, so that the currents generated in both cells are equal and coincide with their respective maximum power points. Once fabricated, the 2T cell cannot be re-optimised, so changes in device properties or external factors over time may result in electrical mis-match. However, if sub-cells are electrically uncoupled in a *four-terminal* (4T) device their operating points are independently controllable, enabling maximum electrical power transfer from each cell at all times. A schematic of the 4T connection is shown in Fig. 1(b).

The properties and potential advantages of 4T-connection in silicon-based solar cells were first explored in detail by Hamakawa [4]. Subsequently Madan [5] analysed prototype 4T micromorph structures, and outlined possible production methods. Dadouche *et al* [6] conducted a computer simulation study of 4T cells with a polymorphous silicon top-cell. They used a numerical solution of the semiconductor device equations, enabling model parameters such as defect density and top-cell layer thickness to be adjusted. Hudanski *et al* [7] conducted outdoor tests on 4T cells and report significant benefits, especially at low light levels. The present authors used semi-empirical modelling [8] to compare the effects of light-induced degradation on 2T and 4T cells. These studies support the view that the greater flexibility of 4T connection may mitigate the impact of sub-optimal matching on energy yield.

Variations in spectral content of sunlight are frequently experienced on a daily cycle, and less obviously, over the seasons. For example, at dawn or dusk sunlight may contain a relatively large proportion of red light. Assuming the tandem cell has been optimized for AM1.5G conditions, an additional fraction will tend to pass through the top-cell and generate an increased current in the bottom-cell. In 2T connection the electrical power deliverable to an external load thus becomes limited by the top-cell. Similarly, if the spectrum contains a larger blue fraction, such as under cloudy conditions, then the tandem becomes bottom-cell limited. In 4T connection no such restriction applies, and provided the maximum-power point for each sub-cell is properly tracked electrical matching will remain optimal.

Here we investigate the impact of variations in solar spectral quality on 2T and 4T connected micromorph solar cells by computer simulation. The solar spectral content, quantified by the average photon energy (*APE*), is varied systematically over the range normally encountered in service. We calculate the short-circuit currents generated by top and bottom cells as a function of *APE* by numerical integration. These currents scale the *J-V* characteristics of reference cells, which are then manipulated to predict relative changes in performance of tandem cells in 2T and 4T connection under varying spectral conditions. Variations in fill-factor due to mis-match, as well as current limitation, are calculated and taken into account, providing a more accurate prediction than reported previously [9]. Finally, statistical frequency distributions of *APE* are used to estimate outdoor performance.

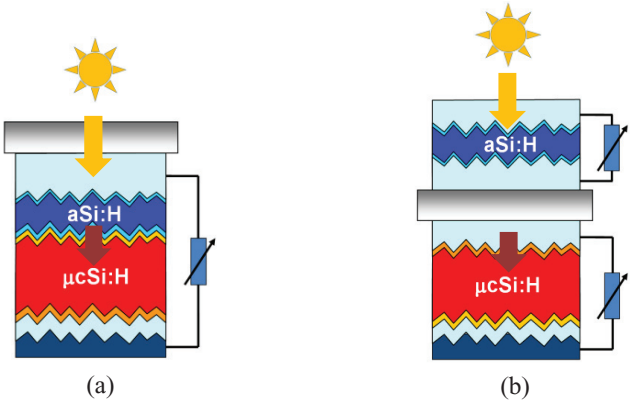

Fig. 1. Schematic representations of (a) two-terminal, (b) four-terminal tandem p-i-n a-Si:H/µc-Si:H solar cells. In (b), a transparent insulating substrate electrically separates the sub-cells. As the specific properties of the substrate and additional TCO layers are not included in the analysis, spectral effects are evaluated as relative changes in performance for each configuration separately.

2. Experimental

Single-junction cell and tandem-cell reference samples were prepared on Corning borosilicate glass substrates coated with 550 nm thick textured ZnO [10] front contact. The semiconductor films were deposited in p-i-n (or p-i-n-p-i-n) sequence by plasma-enhanced chemical vapour deposition from a silane + hydrogen process gas onto the substrate held at 200 – 250 °C. p- and n-layers were doped by introduction of trimethylboron or phosphine respectively, and were 10 – 20 nm thick. For amorphous cells a wider band-gap SiC:H formulation was used as p-layer, to improve blue light transmission. The absorber (i-) layers for single-junction amorphous and microcrystalline silicon cells used here were 280 nm and 1150 nm respectively, and for the tandem cell, 315 nm and 1100 nm respectively The back-contact consisted of a 70 nm layer of ZnO followed by 200 nm Ag squares of dimensions 1 cm × 1 cm. Process details and characterization are described more fully elsewhere [11].

EQE measurements on top and bottom cells, used in the calculation of short-circuit current, are shown in Fig. 2. The amorphous silicon single-junction cell *J-V* curve, used in our simulation to represent the top-cell of the tandem was measured under direct AM1.5G illumination. The microcrystalline silicon bottom-cell was measured when illuminated through an OG590 filter, representing the optical absorption of the top-cell. Both are shown in Fig. 3.

3. Model development

3.1. Solar spectral quality

We express solar spectral quality in terms of the average photon energy *APE*:

$$APE = \frac{\int_{\lambda_1}^{\lambda_2} E(\lambda)d\lambda}{q\int_{\lambda_1}^{\lambda_2} \phi(\lambda)d\lambda}, \tag{1}$$

where $E(\lambda)$ is the irradiance per unit wavelength, and $\phi(\lambda) = E(\lambda)/(hc/\lambda)$ is the corresponding photon flux. λ_1 and λ_2 are the short and long wavelength limits of the spectrum, taken to be 350 and 1050 nm respectively, for consistency with much of the literature. Within these limits, the AM1.5G spectrum has an *APE* of 1.88 eV.

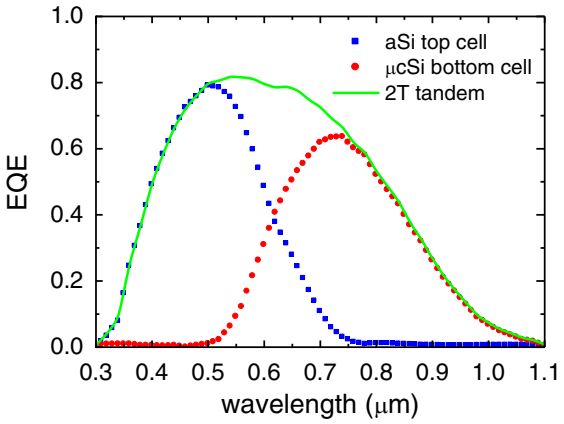

Fig. 2. External quantum efficiency (*EQE*) *vs*. wavelength for top and bottom cells of the 2T tandem cell studied here. The calculated current densities under AM1.5G spectrum are 10.9 and 11.8 mA/cm^2, respectively.

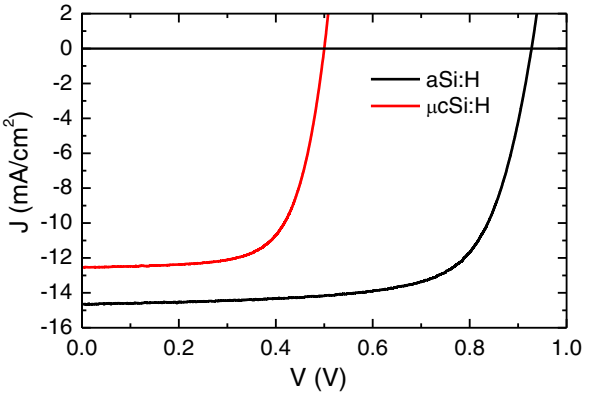

Fig. 3. *J-V* characteristics of single-junction cells studied here. Top-cell: V_{OC} = 0.927 V, J_{SC} = 14.66 mA/cm^2, *FF* = 70.6 %, P_{MPP} = 9.60 mW/cm^2. Bottom-cell: V_{OC} = 0.500 V, J_{SC} = 12.55 mA/cm^2, *FF* = 68.3 %, P_{MPP} = 4.29 mW/cm^2.

We have previously demonstrated [9] that model solar spectra similar to typical measured daily examples at various times of the year in western Europe [12] may be generated by applying a linearly-weighted filter function to the AM1.5G spectrum, defined as:

$$F(\lambda,k) = G(\lambda,k)/G_0(k), \tag{2}$$

where

$$G(\lambda,k) = 1 + k(\lambda - \lambda_0)/\lambda_0 \text{ and} \tag{3}$$

$$G_0(k) = \frac{\int_{\lambda_1}^{\lambda_2} [G(\lambda,k)].[E_{AM1.5G}(\lambda)]d\lambda}{\int_{\lambda_1}^{\lambda_2} E_{AM1.5G}(\lambda)d\lambda}. \tag{4}$$

In this work the filter was pivoted around λ_0 = 630 nm. $G_0(k)$ is a normalizing factor close to unity, which ensures that the total applied optical power per unit area remains constant for all *k*, and equal to the AM1.5G value. Thus only the spectral quality is modified by *k*. The sign of *k* defines whether red (positive) or blue (negative) spectral bias is applied. It is found empirically that *APE* = 1.88 – 0.15*k* eV. Representative spectra are shown in Fig. 4.

It is well-known that spectra which differ in 'shape' and total irradiance may have similar *APE* values [13], this being one of several factors leading to scatter in outdoor data. The approach described here generates a restricted set of spectra, which may have some bearing on our results and is currently under investigation.

3.2. Cell current density

For a given value of *APE*, the short-circuit current density for each sub-cell may be obtained by numerical integration of equation 5. The EQE and spectral data are those illustrated in Figs. 2 and 4 respectively.

$$J_{SC}(k) = q\int_{\lambda_1}^{\lambda_2} [F(\lambda,k)].[\phi_{AM1.5G}(\lambda)].[EQE(\lambda)]d\lambda \cdot \tag{5}$$

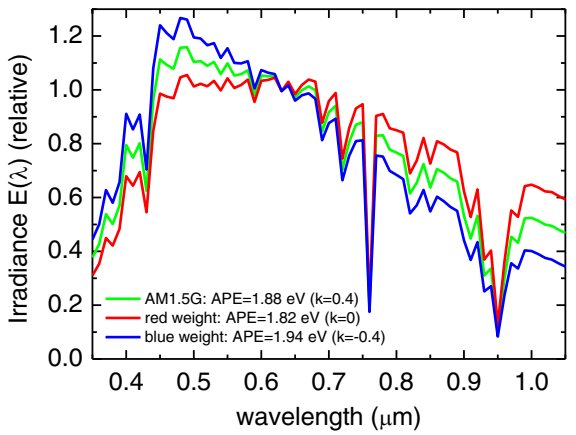

Fig. 4. Spectral weighting introduced by linear scaling function $F(\lambda,k)$ applied to AM1.5G.

3.3. Modelling of 2T and 4T tandem cells

The modelling procedure assumes fundamentally that the *J-V* characteristics of top- and bottom-cells in the tandem cell, which cannot normally be measured directly *in situ*, are similar in shape to the single-junction cell reference curves. The J_{sc} values calculated from equation 5 serve to align each curve at the correct short-circuit current for the prevailing spectral conditions, by adding or subtracting a constant. This shifts the entire curve along the current axis. It is then straightforward to calculate the *J-V* characteristic for 2T series connection, by adding the voltages of top and bottom cells recorded at the same current value. This is facilitated by interpolating each sub-cell curve in equal current steps of 0.05 mA/cm^2. The 2T tandem curve thus obtained is then used to calculate PV parameters under 2T connection. The total electrical power delivered under 4T connection is obtained separately, by summing the individual contributions from top and bottom cells, when each operates at its unconstrained maximum power point.

This model does not take into account optical losses in the insulating slab, and optical and electrical losses in additional TCO layer(s) required in 4T connection, both of which will tend to reduce performance. Differing reflective properties and electrical quality of junctions and interfaces between 2T and 4T connections and single-junction cells may also be significant. Thus we stress that the model is unable to predict absolute efficiencies, in either 2T or 4T connection, and therefore relative changes in spectral performance for each connection separately are discussed. There may also be more subtle effects on the *J-V* and *EQE* curves due to spectrally-induced changes in generation-recombination profiles and field distributions.

4. Results and Discussion

4.1. Verification of 2T J-V characteristics

If the method described above is to be useful, it should be able to reproduce the 2T tandem cell *J-V* characteristic measured under AM1.5G conditions, from the single-junction cell reference curves. The measured and simulated curves are shown in Fig. 5(a). It can be seen that the simulation is similar to the measured curve. Statistical variations across the substrate for the a-Si:H single-junction cells were measured to be ±0.4% for J_{SC}, ±0.3% for V_{OC} and ±1.5% for *FF*, for the μc-Si:H single-junction cells ±2% for J_{SC}, ±1% for V_{OC} and ±3% for *FF*, and for the

tandem cells ±2% for J_{SC}, ±0.3% for V_{OC} and ±2% for *FF*. Discrepancies between the corresponding parameters for the measured and simulated 2T tandem curves are commensurate with the statistical variations. Losses in the recombination junction are not taken into account in our 2T simulation, which could increase the value of *FF*.

J-V curves obtained from modelling mis-matched 2T tandem cells (bottom-cell limited in this example) are shown in Fig. 5(b). The top- and bottom-cell currents are generated under constant power conditions, using the procedure described in section 3. It is evident that as the degree of mis-match is increased, the fill-factor *FF* also increases. This can be understood qualitatively as follows.

When the component cells are current-matched, the equal-current solution yielding the 2T curve embodies the 'knee' part of the characteristic from both top and bottom cells, giving a rounded and gradual rise in current as the forward voltage is increased. If however the top-cell generates more current than the bottom-cell, then the 2T curve will resemble the bottom-cell *J-V* curve in shape, but shifted along the voltage axis by something approaching the open-circuit voltage of the top-cell. The 'knee' in this case is primarily that of the bottom cell alone, giving a sharper increase in current, since the top-cell cannot operate in this region of its characteristic due to the current limit. Overall this results in a more rectangular curve, and a higher *FF*. Assuming that the fill-factors associated with each sub-cell are similar, a more pronounced increase in *FF* in the 2T combination will occur when the sub-cell with the larger open-circuit voltage produces the greater current.

4.2. Relationship between mis-match and 2T PV parameters

The relationship between current mis-match and the PV parameters of the simulated 2T cell is plotted in Fig. 6. Compared with changes in current and fill-factor, changes in open-circuit voltage are a minor effect and are not considered here. Two important features should be noted: (i) maximum power does not correspond to maximum current, (ii) the power vs. mis-match current curve is quite broad. These relationships were measured experimentally by Ulbrich *et al* [14, 15] using an IR and a blue LED to bias the AM1.5G spectrum and thereby mis-match a 2T cell. Our simulated results are quite similar to their experimental curves. This provides useful support for our simulation method. Light-biasing techniques have recently been used with considerable success to probe the individual properties of sub-cells in 2T tandem cells [16, 17].

The results presented in sections 4.1 and 4.2 above address the electrical properties of the 2T tandem cell in terms of the mis-match current, rather than APE. However when outdoor operation is considered, spectral changes are of greater interest. The two quantities may be inter-converted under the specific conditions of this study by the following empirical relation [9]: Mis-match current density = 24 × (*APE* – 1.92), where the current density is expressed in mA/cm^2 and *APE* is in eV.

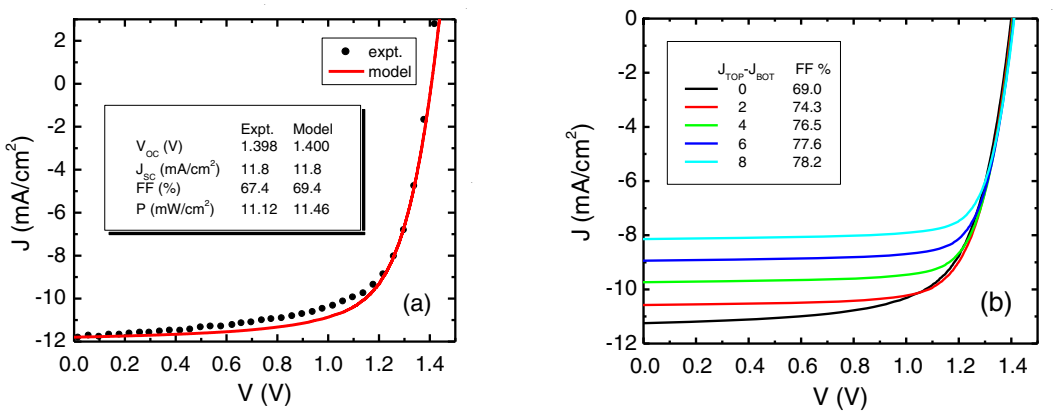

Fig. 5. (a) Comparison of experimental 2T tandem cell and simulated *J-V* curves; (b) Series of simulated *J-V* curves with varying degrees of current mismatch.

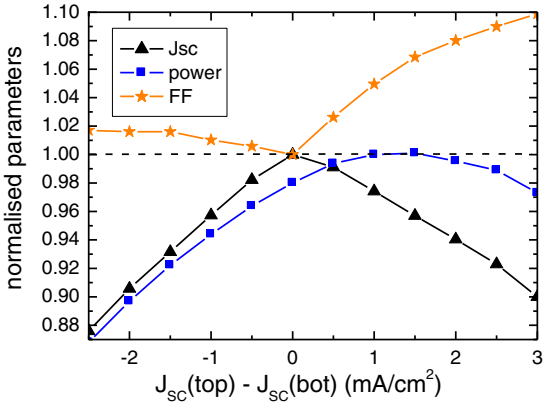

Fig. 6. 2T solar cell simulated parameters vs. current mis-match.

4.3. PV efficiency under 2T and 4T connections, vs. APE

Fig. 7 shows a plot of PV efficiency, normalized relative to the current-matched condition, *vs. APE* for 2T-connected and 4T-connected tandems comprising identical cells, within the model assumptions (see section 3.3). In 4T connection, there is a linear increase in efficiency with increasing *APE* as the increase in power delivered by the top-cell exceeds the decrease in the bottom-cell. On the other hand, the 2T-connected tandem cell shows a pronounced peak in efficiency, a direct consequence of the limitations imposed by electrical matching discussed in section 4.2. In this case, current-matching occurs at an *APE* of 1.92 eV, with the efficiency for both cells normalised at 1.0. Power-matching occurs at an *APE* of 1.96 eV, with a normalised efficiency of 1.013 in 2T connection, and 1.028 in 4T connection. Thus for tandems whose sub-cells are closely matched for a given spectrum, the relative benefit of 4T connection is, predictably, quite small. However, factors such as temperature variations, and reversible and irreversible degradation [18] may result in additional current mismatch, and 2T electrical losses will increase as a result. 4T connection would minimize the impact of degradation on electrical mismatch, although of course conversion efficiency of the top-cell is still reduced [5].

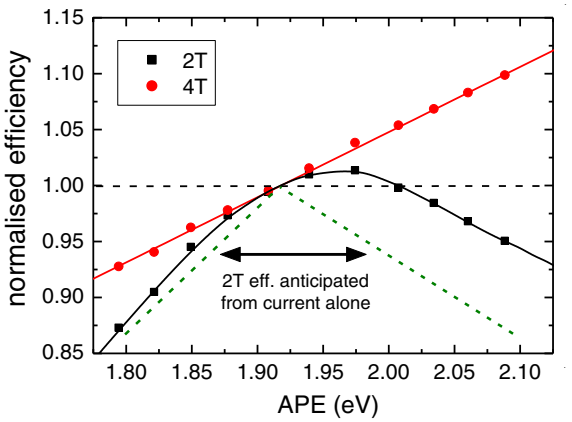

Fig. 7. 2T and 4T tandem cell efficiency curves, *vs. APE*.

Also shown in Fig. 7 is the hypothetical 2T conversion efficiency curve if *FF* is assumed, incorrectly, to remain constant. This curve is much sharper, and would result in more noticeable consequences as irradiance contributions at lower and (particularly) higher *APE* contribute less to annual energy production. Thus, the increase in *FF* highlighted in Fig. 6 may be said to compensate to an extent for loss of external current due to spectral mis-match.

4.4. Effect of outdoor spectral variations

How much electrical energy is lost to spectral mismatch in a 2T tandem cell over its lifetime is related to the distribution of solar irradiance with *APE* at the site. As air-mass is a major influence on the solar spectrum, seasonal latitude-dependent cycles in *APE* are well-known, and so the observation period upon which the distribution is based should comprise at least one, or ideally several, complete years. Fig. 8 shows the distributions of solar irradiance *vs. APE* for three locations (Loughborough (UK), Golden (Colorado USA), and Kusatsa City (Japan)), taken from the literature [13, 19]. While the distributions differ considerably in detail, from the point of view of this work their overall similarity is perhaps of greater importance. Each distribution has a well-defined peak and a full-width at half maximum of around 0.06 eV. The Loughborough distribution (LD) has more extensive 'tails'. The narrowness of the distributions, relative to the 2T efficiency curve shown in Fig. 7, suggests that provided the 2T tandem cell is power-matched for operation at the peak of the energy *vs. APE* distribution the loss in electrical energy due to spectral mismatch in outdoor operation will be modest. To examine this quantitatively, we have taken LD as a template and calculated what might be termed an 'annual average' efficiency η_{AA}. Firstly, the LD was shifted along the *APE* axis to align it at a given *APE*. The integral of the product of the LD and the efficiency curves shown in Fig. 7 was then calculated, and divided by the integral of the LD to give η_{AA}. The procedure was carried out for both 2T and 4T efficiency curves, over an *APE* range from 1.8 to 2.1 eV, and is plotted in Fig. 9. Data in Fig. 7 and Fig. 9 were normalised by dividing by the same efficiency factor, and therefore it is legitimate to compare the effect of the LD on 2T and, separately, 4T connections. For 2T connection η_{AA} is reduced by 0.02 units relative to the peak in Fig. 7. This occurs because each side of the LD is being converted at a lower efficiency than the peak. For 4T connection, the normalised efficiency is also slightly reduced (a parallel shift of 0.01), due to the asymmetry of the LD in favour of the low *APE* side. Greater potential benefit could be derived from 4T connection if top- and-bottom cells were significantly mis-matched to the prevailing long-term average energy distribution.

There have been a number of studies of spectral matching in 2T thin-film silicon tandem solar modules outdoors [19-21]. These are scientifically challenging, because correlations between the variables of *APE*, temperature, irradiance, and light-induced degradation/annealing cycles are difficult to decouple [18]. Minemoto *et al* [19] measured the efficiency of an amorphous/microcrystalline silicon 2T tandem module over a period of one year. A

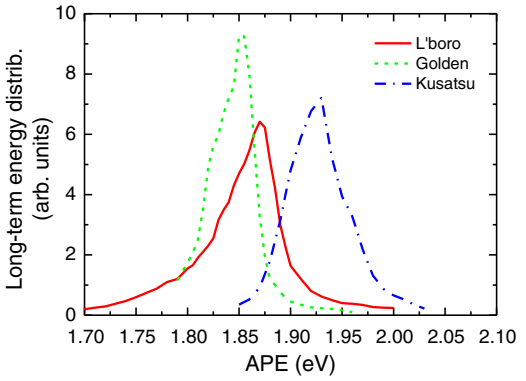

Fig. 8. Long-term radiant energy distribution vs. *APE*, for three global locations.

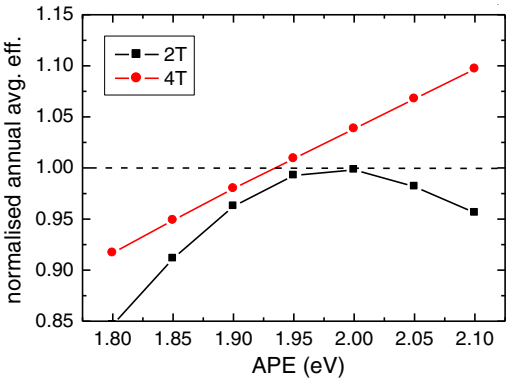

Fig. 9. 'Annual average' PV efficiency *vs*. *APE* calculated using Loughborough irradiance distribution, as explained in text.

plot of the normalized efficiency vs. *APE* shows considerable scatter, but a diffuse peak can be discerned with a maximum at around 1.93 eV. The variation in efficiency 0.05 eV either side of this peak is about 6% of the peak value. The variation predicted by our 2T model is rather smaller, at about 3%. Gottschalg *et al* [20] have reported similar behaviour in amorphous silicon double junctions. Therefore there is evidence that multi-junction modules in 2T connection outdoors undergo measureable losses due to current limitation, of a similar size to our prediction.

Finally, we return to the *APE* curves shown in Fig. 8. The peaks of the distributions measured in Loughborough, Golden and Kusatsa are 1.870, 1.846 and 1.923 eV respectively. However it should be noted that the spectral bandwidth for the first two data sets is from 300 to 1100 nm, and for the third it is 350 to 1050 nm. The *APE* values of AM1.5G measured under these bandwidths are 1.86 and 1.88 eV, respectively. Thus aligning the first two sets with the third requires an upward shift of 0.02 eV, giving 1.890, 1.866 and 1.923 eV respectively. These values span a range similar to the width of the individual *APE* curves, suggesting that spectral shift due to a combination of latitude and prevailing weather conditions may be comparable to spectral distributions at a given site. Significant departures from AM1.5G have been reported for sites studied in France and Algeria [21] (relative redness) and Thailand [22] (strongly asymmetric, and relatively blue).

5. Conclusions

A semi-empirical method has been used to simulate the current-voltage characteristics of a 'micromorph' tandem solar cell, under spectral weightings quantified by the average photon energy. This has enabled the spectral performance of two- and four-terminal electrical connections to be compared separately. For the two-terminal connection, the simulation predictions agree quite well with published laboratory results obtained using light bias, and highlight the distinction between short-circuit current matching and maximum power transfer matching. Simulations have been used in conjunction with outdoor solar energy spectral distribution data to predict the long-term performance of two-terminal and four-terminal connections. Provided the two-terminal tandem is power-matched to the peak of the distribution, the reduction in efficiency relative to a constant solar spectrum is around 2%, or for a 10% efficient cell, 0.2%. The four-terminal connected tandem cell is less affected. If the two-terminal tandem cell is not closely power-matched to the prevailing spectrum, greater comparative benefit is possible. This might occur where a tandem cell optimised for operation under the AM1.5G spectrum is deployed at a site where the spectral distribution differs significantly from this standard, or if the amorphous silicon top-cell undergoes large seasonal degradation and annealing cycles. Further work is required to determine if the potential benefits of four-terminal connection justify the additional processing, energy costs and electrical and optical losses accrued.

Acknowledgements

The authors are grateful for the assistance of Andreas Lambertz, IEK-5, Forschungszentrum Jülich, in preparing and characterizing some of the samples used in this work.

References

[1] Shah AV, Schade H, Vanecek M, Meier J, Vallat-Sauvain E, Wyrsch N, Kroll U, Droz C, Bailat J. Thin-film silicon solar cell technology. *Progress in Photovoltaics: Research and Applications* 2004;**12**:113-142.

[2] Green MA. Third Generation Photovoltaics: Advanced Solar Energy Conversion. Berlin, Germany: Springer; 2006. Chapter 5.

[3] Schicho S, Hrunski D, Van Aubel R, Gordijn A. High potential of thin (< μm) a-Si: H/μc-Si:H tandem solar cells. *Progress in Photovoltaics: Research and Applications* 2012;**18**:83-89.

[4] Hamakawa Y (ed). Thin-Film Solar Cells: Next Generation Photovoltaics and Its Applications. Berlin, Germany: Springer; 2004. Chapter 5.

[5] Madan A. Flexible solar cells and stable high-efficiency four-terminal solar cells using thin-film silicon technology. *Materials and Manufacturing Processes* 2007;**22**:412-418.

[6] Dadouche F, Béthoux O, Gueunier-Farret ME, Johnson EV, Roca I Cabarrocas P, Marchand C, Kleider J-P. Comparative study of thin-film silicon tandem structures pm-Si:H/μc-Si:H in system association prospect. EMRS Spring Meeting Symposium B; 2009 Jun 8-12; Strasbourg, France.

[7] Hudanski L, Kasouit S, Francke L, Damon-Lacoste J, Besnier J-F, Roschek T, Ahmed K, Zhao L, Cassagne V, Vermeersch M. Multiterminal structures for improved efficiency a-Si/μc-Si tandem devices. 37th IEEE PVSC; 2011 Jun 19-24; Seattle WA. p 605.

[8] Reynolds S, Ding K, Smirnov V. Comparison of two- and four-terminal thin-film silicon tandem solar cell performance, using a semi-empirical model. 25th European Photovoltaic Solar Energy Conference. 2010 Sept 6-10; Valencia, Spain.

[9] Reynolds S, Smirnov V, Ding K. Modeling spectral matching in two- and four-terminal thin-film silicon tandem solar cells. 24th International Conference on Efficiency, Cost, Optimization, Simulation and Environmental Impact of Energy Systems (ECOS 2011); 2011 July 4-7; Novi Sad, Serbia.

[10] Böttler W, Smirnov V, Hüpkes J, Finger F. Texture-etched ZnO as a versatile base for optical back reflectors with well-designed surface morphologies for application in thin film solar cells. *Physica Status Solidi (A) Applications and Materials* 2012;**209**:1144-1149.

[11] Smirnov V, Das C, Melle T, Lambertz A, Hülsbeck M, Carius R, Finger F. Improved homogeneity of microcrystalline absorber layer in thin-film silicon tandem solar cells *Mater. Sci. Eng. B* 2009;**159:** 44-47.

[12] Krishnan P, Schüttauf JWA, van der Werf CHM, Houshyani Hassanzadeh B, van Sark WGJHM, Schropp REI. Response to simulated typical daily outdoor irradiation conditions of thin-film silicon-based triple-band-gap, triple-junction solar cells. *Solar Energy Materials & Solar Cells* 2009;**93**:691-97.

[13] Betts TE. Investigation of Photovoltaic Device Operation under Varying Spectral Conditions [PhD thesis]. Loughborough, UK: Loughborough University; 2004.

[14] Ulbrich C, Zahren C, Gerber A, Blank B, Merdzhanova Tz, Gordijn A, Rau U. Matching of Silicon Thin-Film Tandem Solar Cells for Maximum Power Output *International Journal of Photoenergy* 2013; **2013**:314097.

[15] Ulbrich C, Zahren C, Noll J, Blank B, Gerber A, Gordijn A, Rau U. 2011 Power matching of tandem solar cells, 26th EUPVSEC; 2011 September 5-9; Hamburg, Germany.

[16] Holovsky J, Bonnet-Eymard M, Boccard M, Despeisse M, Ballif C. Variable light biasing method to measure component I–V characteristics of multi-junction solar cells. *Solar Energy Materials & Solar Cells* 2012;**103:**128–133.

[17] Bonnet-Eymard M, Boccard M, Bugnon G, Sculati-Meillaud F, Despeisse M, Ballif C. Optimized short-circuit current mismatch in multi-junction solar cells. *Solar Energy Materials & Solar Cells* 2013;**117**:120–125.

[18] Virtuani A, Fanni L. Seasonal power fluctuations of amorphous silicon thin-film solar modules: distinguishing between different contributions. *Prog. Photovolt: Res. Appl.* 2014; **22**:208–217.

[19] Minemoto T, Toda M, Nagai S, Gotoh M, Nakajima A, Yamamoto K, Takatura H, Hamakawa Y. Effect of spectral irradiance distribution on the outdoor performance of amorphous Si//thin-film crystalline Si stacked photovoltaic modules. *Solar Energy Materials & Solar Cells* 2007;**91**:120-22.

[20] Gottschalg R, Betts TR, Infield DG, Kearney MJ. The effect of spectral variations on the performance parameters of single and double junction amorphous silicon solar cells. *Solar Energy Materials & Solar Cells* 2005;**85**:415–428.

[21] Mambrini T, Dubois AM, Longeaud C, Badosa J, Haeffelin M, Prieur L, Radivoniuk V. Photovoltaic yield: correction method for the mismatch between the solar spectrum and the reference ASTMG AM1.5G spectrum. *EPJ Photovoltaics* 2015;**6**:60701.

[22] Sirisamphanwong C, Ketjoy N, Rakwichain W, Vaivudh S. Average photon energy under Thailand's climatic condition. *International Journal of Renewable Energy* 2011;**6**:25-29.